Bioactive Materials 3 (2018) 245–249

Contents lists available at ScienceDirect

Bioactive Materials

journal homepage: http://www.keaipublishing.com/en/journals/bioactive-materials/

Corrosion resistance of a novel SnO_2-doped dicalcium phosphate coating on AZ31 magnesium alloy

Lan-Yue Cui [a, 1], Guang-Bin Wei [a, 1], Rong-Chang Zeng [a, *], Shuo-Qi Li [a], Yu-Hong Zou [b], En-Hou Han [c]

[a] College of Materials Science and Engineering, Shandong University of Science and Technology, Qingdao, 266590, China
[b] College of Chemical and Environmental Engineering, Shandong University of Science and Technology, Qingdao, 266590, China
[c] National Engineering Centre for Corrosion Control, Institute of Metals Research, Chinese Academy of Sciences, Shenyang, 110016, China

ARTICLE INFO

Article history:
Received 26 October 2017
Received in revised form
9 November 2017
Accepted 15 November 2017
Available online 20 November 2017

Keywords:
Phosphate coating
Biomaterials
Magnesium alloys
Corrosion
Stannic oxide

ABSTRACT

A SnO_2-doped dicalcium phosphate coating was prepared on AZ31 alloy by means of hydrothermal deposition. The results showed that the coating possessed a globular morphology with a long lamellar crystalline structure and a thickness of approximately 40 μm. The surface of the coating became smooth with an increase additive amount of the SnO_2 nanoparticles. The corrosion current density and hydrogen evolution rate of the coating prepared in presence of SnO_2 were reduced compared to the coating without SnO_2 and the bare AZ31 substrate, indicating an improvement in the corrosion resistance of the SnO_2-doped coating.

1. Introduction

Metallic biomaterials such as stainless steels and titanium alloys play a critical role in orthopedic surgery [1]. However, the human body causes a hostile response to the traditional metallic implants. Magnesium (Mg) and its alloys hold a promise as temporary implants due to their biodegradability and good biocompatibility [1–4]. Therefore, Mg alloys draw a significant attention to scientists in the biomedical field [5–7]. While the restriction of fast corrosion rate of Mg alloys hampers their clinical applications. It is thus important to slow down the degradation rate of the alloys in order to well match the formation rate of the newly formed bone nearby the implants [8].

Calcium phosphate coatings, including tricalcium phosphate (TCP), dicalcium phosphate anhydrous (DCPA) and hydroxyapatite (HA), may be good choices for surface modification on the degradable Mg alloys [9–12]. Particularly, calcium phosphate is the main component of the bone, attributing to its excellent bioactivity and biocompatibility. There are many approaches, i.e., electrodeposition, sol-gel, biomimetic immersion, to obtain the calcium phosphate coating on Mg alloys [13,14]. Song, Zhang and Guan et al. [15–18] has successfully applied calcium phosphate coating on Mg alloys to improve the biocompatibility and corrosion resistance. Moreover, hydrothermal synthesis is often applied to improve the adhesion strength between the calcium phosphate coating and the Mg substrates, due to its low-cost and time-saving [19,20]. In addition, the morphology and crystallization of the coating can be tailored by the hydrothermal parameters [21].

Previous studies [22,23] have suggested that titanium dioxide (TiO_2) can induce the formation of a calcium phosphate layer on Mg alloys. Tin oxide (SnO_2) has a similar crystal structure [24,25] with TiO_2, it is postulated that SnO_2 can have a similar effect to TiO_2 on inducing the formation of the calcium phosphate layer. In addition, nanocrystalline-doped tin dioxide has been reported to exhibit antibacterial activity [26,27]. Thus, we attempted to use SnO_2 nanoparticles to induce the formation of a Ca-P coating on the surface of Mg alloys and thus achieve a novel SnO_2-doped Ca-P coating with improved corrosion resistance and biocompatibility.

* Corresponding author.
E-mail address: rczeng@foxmail.com (R.-C. Zeng).
Peer review under responsibility of KeAi Communications Co., Ltd.
[1] The authors contributed equally to this work.

https://doi.org/10.1016/j.bioactmat.2017.11.001

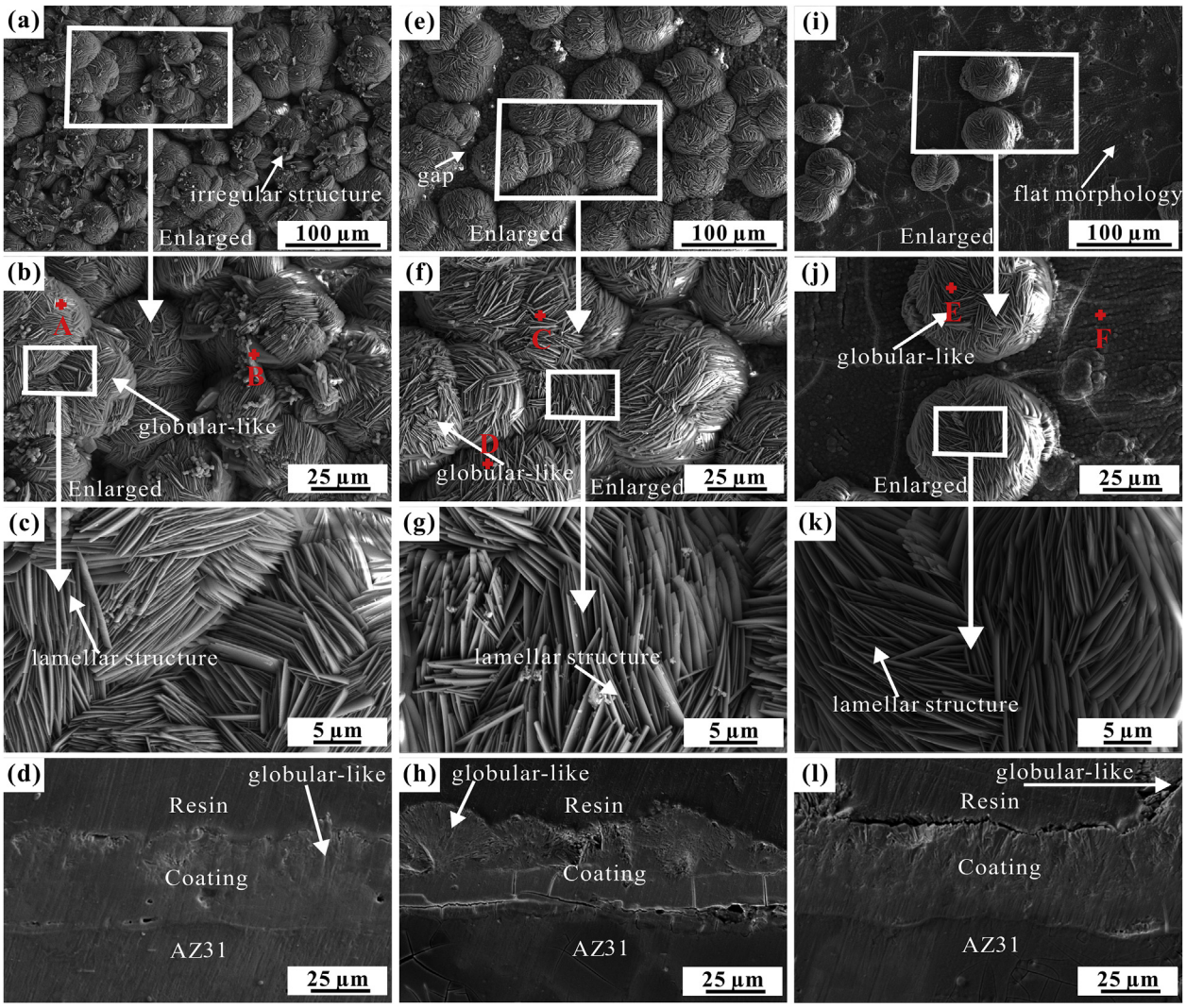

Fig. 1. Surface morphology and cross-sectional images of the coatings: (a–d) in absence of SnO_2, in presence of (e–h) 5 g L^{-1} and (i–l) 10 g L^{-1} SnO_2.

2. Experimental

2.1. Preparation of coatings

As-extruded AZ31 substrates were cut into squares with dimensions of 20 mm × 20 mm × 5 mm, and then ground with SiC papers up to 1500 grit, washed with alcohol and hot dried in air. A hydrothermal synthesis was conducted on the prepared AZ31 samples in a solution with 125 mM ethylenediaminetetraacetic acid disodium salt (Na-EDTA: $C_{10}H_{14}N_2Na_2O_8 \cdot 2H_2O$), 254 mM calcium nitrate ($Ca(NO_3)_2 \cdot 4H_2O$) and 128 mM sodium dihydrogen phosphate ($NaH_2PO_4 \cdot 2H_2O$) together with 33.2 mM (5 g L^{-1}) or 66.4 mM (10 g L^{-1}) SnO_2 nanoparticles (50–70 nm in diameter) at a pH value of approximately 2.9. Then the solution and the samples were transferred into 100 mL Teflon-lined stainless reactors, which were kept in an electric oven (DHG-9070A, China) at a temperature of 100 °C for 20 h. Finally, the samples were taken out and washed thoroughly with distilled water for at least three times and dried with warm air. All the regents were of analytical grade and distilled water was used in all of the experiments.

Table 1
EDS spectra of the coatings on AZ31 Mg alloy, at.%.

Spectrum	C	O	P	Ca	Mg	Ca/P ratio
Point A	13.59	65.51	11.61	9.1	0.19	0.78
Point B	12.49	70.04	9.75	7.49	0.23	0.77
Point C	11.89	64.39	13.21	10.37	0.15	0.79
Point D	14.57	65.57	9.93	8.94	0.99	0.90
Point E	9.47	62.79	14.70	12.86	0.18	0.87
Point F	10.09	55.09	15.65	16.67	1.50	1.07

2.2. Surface analysis and corrosion testing

The phase and morphology of the samples were characterized using X-ray diffraction (XRD, Model D/max 2500PC Rigaku, Japan) and field emission scanning electron microscopy (FE-SEM, Nova Nano SEM 450, USA), respectively. The corrosion behavior was investigated in Hank's solution without any changed during the immersion (8.0 g L^{-1} NaCl, 0.4 g L^{-1} KCl, 0.14 g L^{-1} $CaCl_2$, 0.35 g L^{-1} $NaHCO_3$, 1.0 g L^{-1} glucose ($C_6H_6O_6$), 0.1 g L^{-1} $MgCl_2 \cdot 6H_2O$, 0.06 g L^{-1} $MgSO_4 \cdot 7H_2O$, 0.06 g L^{-1} KH_2PO_4 and 0.06 g L^{-1} $Na_2HPO_4 \cdot 12H_2O$). The ratio of the sample surface area to solution volume was 1: 45 cm^2 mL^{-1}, and the temperature was controlled at 37 ± 0.2 °C by a water bath. The electrochemical corrosion behavior was obtained by an electrochemical analyser (PAR Model 2273,

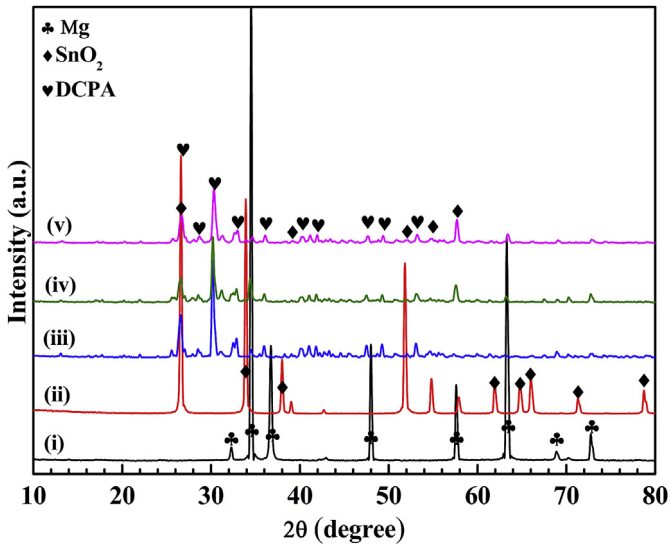

Fig. 2. XRD patterns of the (i) AZ31 substrate, (ii) SnO_2, (iii) coating in absence of SnO_2, coating in presence of (iv) 5 g L^{-1} and (v) 10 g L^{-1} SnO_2.

Princeton, USA). A three-electrode cell set-up was used in which the prepared sample was the working electrode and a platinum sheet and a saturated calomel electrode were used as the counter and reference electrodes, respectively. Electrochemical impedance spectroscopy (EIS) studies were performed at a disturbing potential of 10 mV over a frequency range of 100 kHz to 0.01 Hz at OCP. Then, the potentiodynamic polarization was performed from approximately −2000 to −1000 mV/SCE at a scan rate of 1 mV s^{-1}. The hydrogen evolution was carried out by placing the sample under an inverted funnel, which was connected to a graduated burette [28]. The detailed process was recorded in our previous study [29–31].

3. Results and discussion

Fig. 1 exhibits the surface and cross-sectional SEM morphologies of the coatings prepared by different conditions. The different elemental contents and Ca/P ratio for the samples are shown in Table 1. It is found that the coating in absence of SnO_2 contains a large number of globular structures (Fig. 1a and b). In the globular structures, thin lamellas interlocks together (Fig. 1a–c). The cross-sectional image (Fig. 1d) discloses that the coating has a thickness of approximately 39.95 ± 0.42 μm and a three-layer structure: (I) the inner layer is very thin and connects with the substrate closely; (II) the mid-layer is much thicker than the inner layer; (III) the outer layer is composed of the globular structures with a thickness close to the mid-layer. Several pores are observed in the middle of mid-layer and along the mid-layer/substrate interface.

When the coating doped with 5 g L^{-1} SnO_2 nano-particles, the globular morphology still exist, but the number of globular structures declines, and the gaps between thin lamellas enlarge (Fig. 1e–g). Note that the coating has a thickness of about 39.46 ± 0.57 μm and a three-layer structure, similar to the coating without SnO_2 (Fig. 1h). However, there are many micro-cracks vertical to and along the mid-layer/substrate interface. Larger pores are discerned along the mid-layer/substrate interface. The outer layer has a rougher surface with 5 g L^{-1} SnO_2 than that of the coating in absence of SnO_2. More pores exist in the outer layer.

While doped with 10 g L^{-1} SnO_2, the coating exhibits a flat morphology with few large globular structures randomly distributed on the coating surface (Fig. 1i). It is found that the globular structures are very similar to that in Fig. 1f and g. From the cross-sectional image of the coating (Fig. 1l), it is clear that the coating has a thickness of 43.69 ± 0.36 μm and also a three compact layers: very thin inner layer, thick mid-layer and thicker outer layer. There are no evident micro-cracks and pores in the whole coating, indicating the good adhesion of the coating to the substrate. The Ca/P ratio increases up to about 1.0 with the addition of the SnO_2 nano-particles. That is, the main composition of the SnO_2 doped Ca-P coating may be $CaHPO_4$ (DCPA) or $CaHPO_4 \cdot 2H_2O$ (DCPD).

Fig. 2 shows the XRD patterns of the samples. Except for α-Mg diffraction peaks, the major diffraction peaks are DCPA [32], indicating that the DCPA coatings are successfully deposited on the Mg alloys by hydrothermal deposition methods. Furthermore, SnO_2 diffraction peaks, particularly at 2θ of 26° and 58° are observed for both Fig. 2(iv) and (v). Moreover, the relative intensity of diffraction peaks of SnO_2 in Fig. 2(v) are higher than that in Fig. 2(iv), suggesting that the SnO_2 are successfully deposited in the coating. The more content the SnO_2 nanoparticles, the higher the peak intensity.

In general, proper compactness and thickness endow protective coatings with favorable corrosion resistance for Mg alloys [33]. In order to evaluate the protective effects of the obtained Ca-P coatings, potentiodynamic polarization and EIS tests are conducted in Hank's solutions and the results are shown in Fig. 3. Theoretically, the lower current density (i_{corr}) and higher corrosion potential (E_{corr}) indicate the better corrosion resistance [34]. The i_{corr} of the DCPA coating without SnO_2 is 7.04 × 10^{-6} A cm^{-2}, which is about

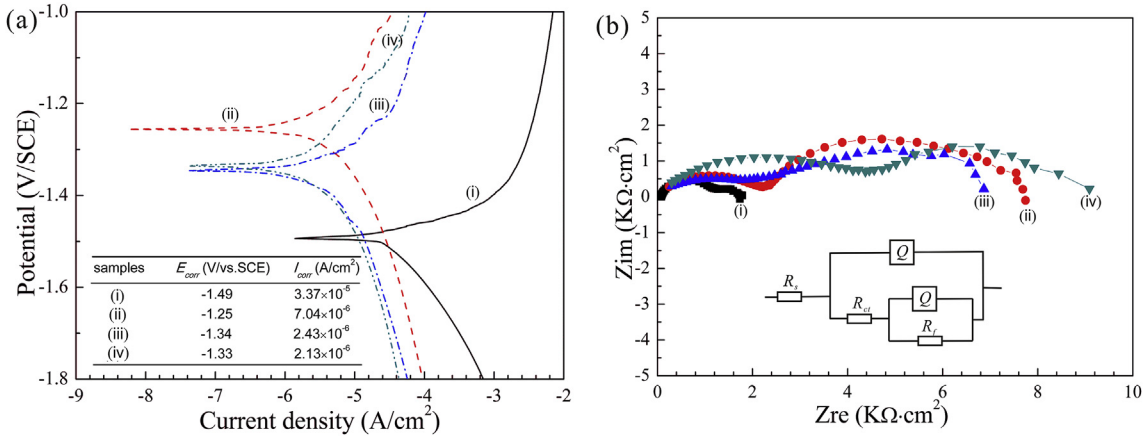

Fig. 3. The (a) polarization curves and (b) Nyquist plots of the (i) AZ31 Mg alloy, (ii) coating in absence of SnO_2, coating in presence of (iii) 5 g L^{-1} and (iv) 10 g L^{-1} SnO_2.

Table 2
Electrochemical data obtained via equivalent circuit fitting of the EIS curves.

Samples	R_s ($\Omega \cdot cm^2$)	Q_1 ($\Omega^{-1} \cdot s^n \cdot cm^{-2}$)	n_1	R_{ct} ($\Omega \cdot cm^2$)	Q_2 ($\Omega^{-1} \cdot s^n \cdot cm^{-2}$)	n_2	R_f ($\Omega \cdot cm^2$)
AZ31 substrate	78.07	1.86×10^{-5}	0.87	1153	1.42×10^{-3}	0.90	465
DCPA coating	71.07	6.21×10^{-7}	0.62	2254	5.92×10^{-5}	0.70	5464
5 g L^{-1} DCPA coating	93.78	1.23×10^{-6}	0.56	2046	5.65×10^{-5}	0.50	5648
10 g L^{-1} DCPA coating	99.71	5.25×10^{-7}	0.61	4298	4.21×10^{-5}	0.61	4793

4.8 times lower than that (3.37×10^{-5} A cm^{-2}) of the AZ31 substrate. The i_{corr} of the DCPA coating prepared with 5 g L^{-1} SnO_2 is 2.43×10^{-6} A cm^{-2}, which is approximately 2.9 times lower than that of the DCPA coating prepared without SnO_2. Although the i_{corr} of the DCPA coating with 10 g L^{-1} SnO_2 (2.13×10^{-6} A cm^{-2}) is close to that in presence of 5 g L^{-1} SnO_2, the anodic polarization curve of the former is shifted toward the left and has a higher breakdown potential (−1.16 V) than the latter (−1.24 V). The scenario implies that 10 g L^{-1} SnO_2 changes the anodic behavior and improves the corrosion resistance of the coating due to its perfect compactness and higher thickness.

To more accurately explain our results in detail, the appropriate equivalent circuit of samples are shown in Fig. 3b. The fitting data are listed in Table 2. In the equivalent circuit, R_f shows the resistance of the coating. Q_1 and Q_2 represent constant phase elements (*CPEs*). R_s and R_{ct} are the solution resistance and the charge transfer resistance, respectively. A higher R_{ct} means a better corrosion resistance of the alloy. The R_{ct} of the samples can be ranked in: 1153 Ω cm^2 (AZ31 substrate) < 2046 Ω cm^2 (coating with 5 g L^{-1} SnO_2) < 2254 Ω cm^2 (coating without SnO_2) < 4298 Ω cm^2 (coatings with 10 g L^{-1} SnO_2) (Fig. 3b). The consequence is in pronounced agreement with the result of the polarization curves (Fig. 3a) and the cross-sectional images (Fig. 1). The DCPA coating, doped with 10 g L^{-1} SnO_2, has the best corrosion resistance. Note that, the subtle difference in R_{ct} between coating with 5 g L^{-1} SnO_2 and coating without SnO_2 may be ascribed to the presence of the micropores and micro-cracks in the coating prepared with 5 g L^{-1} SnO_2.

Fig. 4 exhibits the curves of hydrogen evolution rates (HER) and SEM images for the samples during and after an immersion of 204 h, respectively. The HERs of the AZ31 Mg alloy, the coating without and with 5 g L^{-1} SnO_2 are very high and decreases significantly in the first 36 h of immersion (Fig. 4i, ii and iii), due to the existence of defects (Fig. 1d and h) in the coatings. After 36 h of immersion, the HER of the samples maintain a stable value and last for about 108 h, indicating the formation of $Mg(OH)_2$ film and Ca-P precipitate on the AZ31 substrate, so that the coatings was self-healed in Hank's solution [2,35]. After 108 h of immersion, the HERs of the AZ31 Mg alloy increases firstly, follows by the coating without SnO_2, and then the coating in presence of 5 g L^{-1} SnO_2. This result can be attributed to the dissolution of $Mg(OH)_2$ film into soluble $MgCl_2$ for the substrate, and the delaminating and peeling-off of the coatings. Note that, the HER of the coating prepared in presence of 10 g L^{-1} SnO_2 maintains a lower value during the immersion time. After 10 days of immersion, the HERs of the AZ31 substrate, the coating without SnO_2, the coatings in presence of 5 g L^{-1} and 10 g L^{-1} SnO_2 can be ranked in: 2.18×10^{-2} > 1.04×10^{-2} > 2.3×10^{-3} > 4.72×10^{-4} mL cm^{-2} h^{-1}. In Fig. 4b, all of samples keep a relatively intact morphology in comparison with Fig. 1, which ascribed to the corrosion protection of the DCPA coating and the formation of $Mg(OH)_2$ film and Ca-P precipitate. The finding demonstrates that the coating doped by 10 g L^{-1} SnO_2 has the best corrosion resistance. This result agrees well with that of the above electrochemical tests.

Moreover, Sn is generally considered as a relatively non-toxic metal. The reason is that Sn and its compounds are poorly absorbed and accumulated in human tissues and that Sn is rapidly excreted mainly by kidneys [36]. Note that, Kubásek et al. [37] demonstrated that a relatively high concentration (2520 ng mL^{-1}) of Sn caused a severe toxic effect on the cells. After twofold dilution of the concentration of Sn, the cell activity was also very low. But when the Sn amount decreased to 163 ng mL^{-1}, the cells remained viable even after 5 days culture. Pan et al. [38] showed that the MG63 cells exhibited good growth in both Mg-1Sn and Mg-3Sn alloy extracts and these alloys met the requirement of cell toxicity according to ISO 10993-5: 1999. Although the degradation rate of the DCPA coating is slow, the security of the released SnO_2 nanoparticles in the coating is an another problem, which should be confirmed further.

In principle, the formation of the DCPA coatings on Mg alloys from the aqueous solution consists of two processes: nucleation and crystal growth [39]. The driving force for the above two processes involve the relative supersaturation [40], which increases

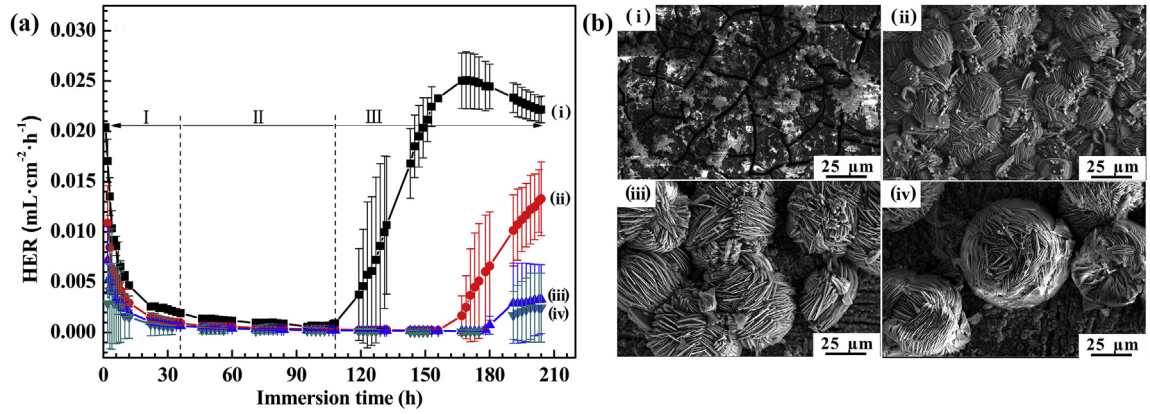

Fig. 4. (a) HERs and (b) SEM images of the (i) AZ31 Mg alloy, (ii) coating in absence of SnO_2, coating in presence of (iii) 5 g L^{-1} and (iv) 10 g L^{-1} SnO_2 with and after an immersion of 204 h in Hank's solutions.

with increasing temperature and pH of the solution [41]. The formation mechanism of the coatings is attributed to the self-assembled EDTA molecules, interfacial molecular recognition and biomineralization [42].

In the hydrothermal deposition, the driving force was considered not high enough, thus lamellar DCPA crystals precipitated, then continuously wrapped and agglomerated into large globules to reduce the overall surface energy [39]. Once the SnO_2 nanoparticles were added into the solution, the SnO_2 nano-particles as a foreign material provided heterogeneous nucleation sites for the deposition of Ca^{2+} and HPO_4^{2-}, and thus promoted the formation of the nuclei, then the surface became flat. Thereby, the deposition process accelerated and the thickness increased duo to the heterogeneous nucleation resulted from the SnO_2 nanoparticles. In addition, the nano-sized SnO_2 particles, filled in the micro-cracks or pores of the coating, thus led to the formation of a denser film.

4. Conclusions

In summary, SnO_2 nano-particles were successfully doped to the DCPA coating on the AZ31 alloys via hydrothermal deposition, resulting in the formation of a thick and dense DCPA coating. The DCPA coating doped with 10 g L^{-1} SnO_2 exhibits an improved corrosion resistance as compared to that of the DCPA coating prepared in absence of SnO_2.

Acknowledgements

This work was supported by the National Natural Science Foundation of China (51571134); and the Research Fund of Shandong University of Science and Technology (2014TDJH104).

References

[1] N. Li, Y. Zheng, Novel magnesium alloys developed for biomedical application: a review, J. Mater. Sci. Technol. 29 (2013) 489–502.
[2] R.C. Zeng, X.T. Li, L.J. Liu, S.Q. Li, F. Zhang, In vitro degradation of pure Mg for esophageal stent in artificial saliva, J. Mater. Sci. Technol. 32 (2016) 437–444.
[3] J. Chen, Y. Song, D. Shan, E.H. Han, In situ growth process of Mg-Al hydrotalcite conversion film on AZ31 Mg alloy, J. Mater. Sci. Technol. 31 (2015) 384–390.
[4] Z. Zhen, T. Xi, Y. Zheng, L. Li, L. Li, In vitro study on Mg-Sn-Mn Alloy as biodegradable metals, J. Mater. Sci. Technol. 30 (2014) 675–685.
[5] M.B. Kannan, R.K.S. Raman, Evaluating the stress corrosion cracking susceptibility of Mg-Al-Zn alloy in modified-simulated body fluid for orthopaedic implant application, Scr. Mater. 59 (2008) 175–178.
[6] J.K. Lin, C.L. Hsia, J.Y. Uan, Characterization of Mg, Al-hydrotalcite conversion film on Mg alloy and Cl^- and CO_3^{2-} anion-exchangeability of the film in a corrosive environment, Scr. Mater. 56 (2007) 927–930.
[7] R.C. Zeng, X.T. Li, S.Q. Li, F. Zhang, E.H. Han, In vitro degradation of pure Mg in response to glucose, Sci. Rep. 5 (2015).
[8] J.E. Gray, B. Luan, Protective coatings on magnesium and its alloys: a critical review, J. Alloys Compd. 336 (2002) 88–113.
[9] B.Y. Chou, E. Chang, Interface investigation of plasma-sprayed hydroxyapatite coating on titanium alloy with ZrO_2 intermediate layer as bond coat, Scr. Mater. 45 (2001) 487–493.
[10] F.Z. Cui, J.X. Yang, Y.P. Jiao, Q.S. Yin, Y. Zhang, I.S. Lee, Calcium phosphate coating on magnesium alloy for modification of degradation behavior, Front. Mater. Sci. 2 (2008) 143–148.
[11] R. Narayanan, S.K. Seshadri, T.Y. Kwon, K.H. Kim, Electrochemical nano-grained calcium phosphate coatings on Ti-6Al-4V for biomaterial applications, Scr. Mater. 56 (2007) 229–232.
[12] Z.Z. Yin, R.C. Zeng, L.Y. Cui, Y.H. Zou, S.Q. Li, F. Zhang, Progress on phosphate coatings on biodegradable magnesium alloys, J. Shandong Univ. Sci. Technol. 36 (2017) 57–69.
[13] F. Li, Q.L. Feng, F.Z. Cui, H.D. Li, H. Schubert, A simple biomimetic method for calcium phosphate coating, Surf. Coat. Technol. 154 (2002) 88–93.
[14] H.K. Varma, Y. Yokogawa, F.F. Espinosa, Y. Kawamoto, K. Nishizawa, F. Nagata, T. Kameyama, Porous calcium phosphate coating over phosphorylated chitosan film by a biomimetic method, Biomaterials 20 (1999) 879–884.
[15] Y. Song, S. Zhang, J. Li, C. Zhao, X. Zhang, Electrodeposition of Ca-P coatings on biodegradable Mg alloy: in vitro biomineralization behavior, Acta Biomater. 6 (2010) 1736–1742.
[16] C.Y. Zhang, R.C. Zeng, C.L. Liu, J.C. Gao, Comparison of calcium phosphate coatings on Mg-Al and Mg-Ca alloys and their corrosion behavior in Hank's solution, Surf. Coat. Technol. 204 (2010) 3636–3640.
[17] C. Wen, S. Guan, L. Peng, C. Ren, X. Wang, Z. Hu, Characterization and degradation behavior of AZ31 alloy surface modified by bone-like hydroxyapatite for implant applications, Appl. Surf. Sci. 255 (2009) 6433–6438.
[18] H. Wang, S. Zhu, L. Wang, Y. Feng, X. Ma, S. Guan, Formation mechanism of Ca-deficient hydroxyapatite coating on Mg-Zn-Ca alloy for orthopaedic implant, Appl. Surf. Sci. 307 (2014) 92–100.
[19] S.K.F. Asl, S. Nemeth, M.J. Tan, Improved corrosion protection of magnesium by hydrothermally deposited biodegradable calcium phosphate coating, Mater. Chem. Phys. 161 (2015) 185–193.
[20] R.C. Zeng, Z.D. Lan, L.H. Kong, Y.D. Huang, H.Z. Cui, Characterization of calcium-modified zinc phosphate conversion coatings and their influences on corrosion resistance of AZ31 alloy, Surf. Coat. Technol. 205 (2011) 3347–3355.
[21] F. Zhang, C.L. Zhang, L. Song, R.C. Zeng, S.Q. Li, H.Z. Cui, Fabrication of the superhydrophobic surface on magnesium alloy and its corrosion resistance, J. Mater. Sci. Technol. 31 (2015) 1139–1143.
[22] X. Shi, L. Xu, Q. Wang, Porous TiO_2 film prepared by micro-arc oxidation and its electrochemical behaviors in Hank's solution, Surf. Coat. Technol. 205 (2010) 1730–1735.
[23] Z.Q. Yao, Y. Ivanisenko, T. Diemant, A. Caron, A. Chuvilin, J.Z. Jiang, R.Z. Valiev, M. Qi, H.J. Fecht, Synthesis and properties of hydroxyapatite-containing porous titania coating on ultrafine-grained titanium by micro-arc oxidation, Acta Biomater. 6 (2010) 2816–2825.
[24] F.Z. Shi, Q.H. Zhang, Y.G. Li, H.Z. Wang, Preparation and characterization of apatite coated rutile TiO_2 composite powders, J. Inorg. Mater. 24 (2009) 893–896.
[25] Y.P. Du, J.C. Chen, J. Feng, Mechanical properties and electronic structures of various SnO_2 crystal structures, Wuli Huaxue Xuebao 25 (2009) 273–287.
[26] S. Haskouri, H. Cachet, J.L. Duval, C. Debiemme-Chouvy, First evidence of the antibacterial property of SnO_2 surface electrochemically modified in the presence of bovine serum albumin and chloride ions, Electrochem. Commun. 8 (2006) 1115–1118.
[27] V.K. Vidhu, D. Philip, Biogenic synthesis of SnO_2 nanoparticles: evaluation of antibacterial and antioxidant activities, Spectrochim. Acta Part A 134 (2015) 372–379.
[28] R.C. Zeng, W.C. Qi, H.Z. Cui, F. Zhang, S.Q. Li, E.H. Han, In vitro corrosion of as-extruded Mg-Ca alloys—the influence of Ca concentration, Corros. Sci. 96 (2015) 23–31.
[29] R.C. Zeng, L.Y. Cui, K. Jiang, R. Liu, B.D. Zhao, Y.F. Zheng, In vitro corrosion and cytocompatibility of a microarc oxidation coating and poly(L-lactic acid) composite coating on Mg-1Li-1Ca alloy for orthopedic implants, ACS Appl. Mater. Interfaces 8 (2016) 10014–10028.
[30] L.Y. Cui, S.D. Gao, P.P. Li, R.C. Zeng, F. Zhang, S.Q. Li, E.H. Han, Corrosion resistance of a self-healing micro-arc oxidation/polymethyltrimethoxysilane composite coating on magnesium alloy AZ31, Corros. Sci. 118 (2017) 84–95.
[31] L.Y. Cui, Y. Hu, R.C. Zeng, Y.X. Yang, D.D. Sun, S.Q. Li, F. Zhang, E.H. Han, New insights into the effect of Tris-HCl and Tris on corrosion of magnesium alloy in presence of bicarbonate, sulfate, hydrogen phosphate and dihydrogen phosphate ions, J. Mater. Sci. Technol. 33 (2017) 971–986.
[32] L.I. Kaikai, W. Bing, B. Yan, L.U. Wei, Preparing Ca-P coating on biodegradable magnesium alloy by hydrothermal method:In vitro degradation behavior, Sci. Bull. 57 (2012) 2319–2322.
[33] Y.K. Pan, C.Z. Chen, D.G. Wang, T.G. Zhao, Effects of phosphates on microstructure and bioactivity of micro-arc oxidized calcium phosphate coatings on Mg-Zn-Zr magnesium alloy, Colloids Surf. B 109C (2013) 1–9.
[34] H. Yu, G. Xu, X. Shen, X. Yan, H. Chen, Y. Wang, Corrosion resistance and infrared emissivity properties of EPDM (EPDM-g-MAH) film on low infrared emissivity PU/Cu coating, Electrochim. Acta 55 (2010) 1843–1847.
[35] R. Zeng, X. Guo, C. Liu, H. Cui, W. Tao, Y. Liu, B. Li, Study on corrosion of medical Mg-Ca and Mg-Li-Ca alloys, Acta Metall. Sin. (Engl. Lett.) 47 (2011) 1477–1482.
[36] Inorganic Tin in Drinking-water, Background Document for Development of WHO for Guidelines Drinking-water Quality, 2004. http://www.who.int/water_sanitation_health/dwq/chemicals/tin. (Accessed 20 February 2013).
[37] J. Kubásek, D. Vojtěch, J. Lipov, T. Ruml, Structure, mechanical properties, corrosion behavior and cytotoxicity of biodegradable Mg-X (X=Sn, Ga, In) alloys, Mater. Sci. Eng. C 33 (2013) 2421–2432.
[38] C. Zhao, F. Pan, S. Zhao, H. Pan, K. Song, A. Tang, Microstructure, corrosion behavior and cytotoxicity of biodegradable Mg-Sn implant alloys prepared by sub-rapid solidification, Mater. Sci. Eng. C 54 (2015) 245.
[39] S. Shen, S. Cai, M. Zhang, G. Xu, Y. Li, R. Ling, X. Wu, Microwave assisted deposition of hydroxyapatite coating on a magnesium alloy with enhanced corrosion resistance, Mater. Lett. 159 (2015) 146–149.
[40] S. Ban, J. Hasegawa, Morphological regulation and crystal growth of hydrothermal-electrochemically deposited apatite, Biomaterials 23 (2002) 2965–2972.
[41] B. Viswanath, N. Ravishankar, Controlled synthesis of plate-shaped hydroxyapatite and implications for the morphology of the apatite phase in bone, Biomaterials 29 (2008) 4855–4863.
[42] C. Mao, H. Li, F. Cui, Q. Feng, C. Ma, The functionalization of titanium with EDTA to induce biomimetic mineralization of hydroxyapatite, J. Mater. Chem. 9 (1999) 2573–2582.